

See discussions, stats, and author profiles for this publication at: <https://www.researchgate.net/publication/265343527>

# Conformational, Spectroscopic, and Molecular Dynamics DFT Study of Precursors for New Potential Antibacterial Fluoroquinolone Drugs

ARTICLE in THE JOURNAL OF PHYSICAL CHEMISTRY A · SEPTEMBER 2014

Impact Factor: 2.69 · DOI: 10.1021/jp506355f · Source: PubMed

CITATION

1

READS

36

## 12 AUTHORS, INCLUDING:



[Lukas Bucinsky](#)

Slovak University of Technology in Bratislava

23 PUBLICATIONS 80 CITATIONS

SEE PROFILE



[Lenka Kuckova](#)

Slovak University of Technology in Bratislava

13 PUBLICATIONS 36 CITATIONS

SEE PROFILE



[Marek Fronc](#)

Slovak University of Technology in Bratislava

36 PUBLICATIONS 59 CITATIONS

SEE PROFILE



[Viktor Milata](#)

Slovak University of Technology in Bratislava

141 PUBLICATIONS 540 CITATIONS

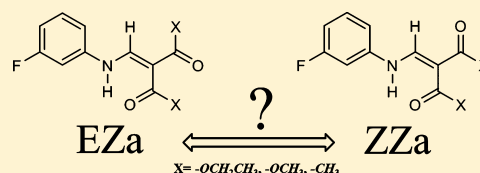
SEE PROFILE

## Conformational, Spectroscopic, and Molecular Dynamics DFT Study of Precursors for New Potential Antibacterial Fluoroquinolone Drugs

Sandra Dorotíková,<sup>†</sup> Kristína Plevová,<sup>‡</sup> Lukáš Bučinský,<sup>\*,†</sup> Michal Malček,<sup>†</sup> Peter Herich,<sup>†</sup> Lenka Kucková,<sup>†</sup> Miroslava Bobeničová,<sup>†</sup> Stanislava Šoralová,<sup>§</sup> Jozef Kožíšek,<sup>†</sup> Marek Fronc,<sup>†</sup> Viktor Milata,<sup>‡</sup> and Dana Dvoranová<sup>†</sup><sup>†</sup>Institute of Physical Chemistry and Chemical Physics, Faculty of Chemical and Food Technology, Slovak University of Technology in Bratislava, Radlinského 9, SK-812 37 Bratislava, Slovak Republic<sup>‡</sup>Institute of Organic Chemistry, Catalysis and Petrochemistry, Faculty of Chemical and Food Technology, Slovak University of Technology in Bratislava, Radlinského 9, SK-812 37 Bratislava, Slovak Republic<sup>§</sup>Department of Pharmaceutical Chemistry, Faculty of Pharmacy, Comenius University in Bratislava, Odbojárov 10, SK-832 32 Bratislava, Slovak Republic

## S Supporting Information

**ABSTRACT:** Biological activity, functionality, and synthesis of (fluoro)-quinolones is closely related to their precursors (for instance 3-fluoroanilinoethylene derivatives) (i.e., their functional groups, conformational behavior, and/or electronic structure). Herein, the theoretical study of 3-fluoroanilinoethylene derivatives is presented. Impact of substituents (acetyl, methyl ester, and ethyl ester) on the conformational analysis and the spectral behavior is investigated. The B3LYP/6-311++G\*\* computational protocol is utilized. It is found that the intramolecular hydrogen bond N–H...O is responsible for the energetic preference of *anti* (a) conformer (*anti* position of 3-fluoroanilino group with respect to the C=C double bond). The Boltzmann ratios of the conformers are related to the differences of the particular dipole moments and/or their dependence on the solvent polarity. The studied acetyl, ethyl ester, and methyl ester substituted fluoroquinolone precursors prefer in the solvent either EZa, ZZa, or both conformers equally, respectively. In order to understand the degree of freedom of rotation of the *trans* ethyl ester group, B3LYP/6-311G\*\* molecular dynamic simulations were carried out. Vibrational frequencies, electron transitions, as well as NMR spectra are analyzed with respect to conformational analysis, including the effect of the substituent. X-ray structures of the precursors are presented and compared with the results of the conformational analysis.



X-ray  
Conformational analysis  
MD simulations  
IR, UV-VIS, NMR

## ■ INTRODUCTION

3-Fluoroanilinoethylene derivatives belong to precursors of quinolones. Quinolones possess a variety of biological activities, including antimicrobial,<sup>1</sup> antiviral (anti-HIV),<sup>2,3</sup> and antimalarial effects.<sup>4</sup> Nowadays, the fluoroquinolones play a specific role in medicine, being widely used for the treatment of infections caused by both Gram-positive<sup>5,6</sup> or Gram-negative<sup>6–8</sup> pathogens. Moreover, fluoroquinolones have been demonstrated to possess antitumor activity,<sup>9,10</sup> hand-in-hand with interesting mechanical effect on the DNA molecule.<sup>11–14</sup> DNA gyrase and DNA topoisomerase IV are both sensitive to the 4-quinolone class of antibacterial compounds in vitro. This activity of quinolones is the result of the inhibition of the supercoiling of DNA catalyzed by the enzyme DNA gyrase. Emami et al.<sup>15</sup> and Shen<sup>16</sup> have proposed drug–DNA models which imply hydrogen-bond type interactions between the DNA unpaired bases and the quinolone, as well as a stacked dimerization of the drug. Stereochemistry is becoming very important in such interactions (i.e., the orientation of the substituents can be critical for the activity of the agents).

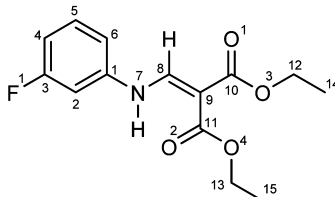
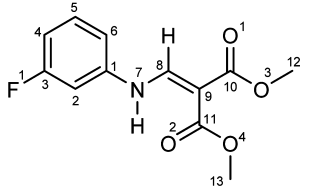
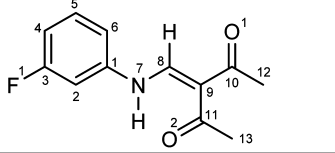
Manipulations of the basic molecule, including replacement of hydrogen with fluorine, substitution on the cyclic amine residue, and the addition of new residues on the quinolone ring, have led to improved breadth and potency of antibacterial activity and pharmacokinetics. Thus, the primary attention was foremostly focused on the investigations of structure–activity relationships of fluoroquinolones. Nowadays, the attention turns to innovative novel reaction pathways which lead to the synthesis of novel derivatives, emphasizing the role of the precursors from which the substances are mainly prepared using the modified Gould-Jacobs reaction.<sup>17,18</sup> Newly synthesized 3-fluoroquinolones have been prepared from precursors bounded with different substituents R<sub>1</sub> and R<sub>2</sub>, such as –COOC<sub>2</sub>H<sub>5</sub>, –COOCH<sub>3</sub>, and –COCH<sub>3</sub>.<sup>19</sup> The structure of these precursors of fluoroquinolones is summarized in Table 1.

Received: June 26, 2014

Revised: September 4, 2014

Published: September 4, 2014

Table 1. Overview of the Fluoroquinolone Precursors under Study

Abbreviation	Structure	Systematic name
P1		diethyl 2-[(3-fluorophenylamino)methylene]malonate
P2		dimethyl 2-[(3-fluorophenylamino)methylene]malonate
P3		3-[(3-fluorophenylamino)methylene]pentane-2,4-dione

---

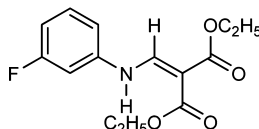
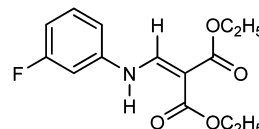
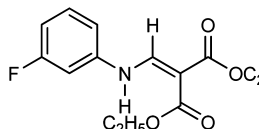
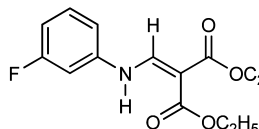
<b>EEa</b>	<b>EZa</b>	<b>ZEa</b>	<b>ZZa</b>
			

Figure 1. Molecular structures of studied anti conformers of P1.

In accordance with the literature data,<sup>20,21</sup> previous quantum-chemical studies were oriented exclusively toward the spectroscopic and tautomeric characterization of quinolones. A closer theoretical study of (fluoro)quinolone precursors using standard DFT computational protocols and a subsequent comparison to the experiment<sup>19</sup> has not been carried out yet. The fluoroquinolone precursors are well-known as push–pull ethylenes.<sup>22–24</sup> Similar push–pull ethylenes prefer the anti (a) orientation of 3-fluoroaniline group with respect to the C=C double bond of ethylene comparing to the syn (s) orientation.<sup>25–27</sup> Intramolecular hydrogen bond between the amino hydrogen and carbonyl oxygen from the acetyl or methyl/ethyl ester group is found to be a key factor for the energetically preferred conformers.<sup>28</sup> Hence, the *E* or *Z* isomers (acetyl/methyl ester/ethyl ester C=O group in the trans or cis position toward the amino group) are the most significant for the conformational analysis of such compounds. Molecular structures of the studied anti conformers are shown in Figure 1. Challenge in these push–pull substituted fluoroquinolone precursors is the admixture of concurrent interactions. The  $\pi$ -conjugation prefers a planar structure of the push–pull systems. The planar structure is furthermore stabilized by the hydrogen bond between the amino hydrogen and the carbonyl oxygen from the acetyl<sup>29</sup> or methyl/ethyl ester<sup>30</sup> group. On the other hand,  $sp^3$  hybridization of the amino nitrogen and the hydrogen–hydrogen repulsion prefer different nonplanar geometries. Hence, these systems are well-suited for a real test of standard computational protocols. In addition, the

biological activity of synthesized (fluoro)quinolones is determined by their precursors, as mentioned above (i.e., their functional groups conformational behavior and/or electronic structure). In general,  $\beta$ -keto carboxylic acid moiety (positions C10 and C11) is essentially required for hydrogen-bonding interactions with DNA. Furthermore, the antibacterial and/or DNA-binding activity as well as pharmacokinetic properties of quinolones depend on the nature of peripheral substituents and their spatial arrangements.<sup>15</sup> The position of the fluorine atom and the orientation of the group which does not undergo the cyclization to quinolone are also directly related to the conformational behavior of the initial precursor and might be directly related to the biological activity of the target quinolone.

Herein, DFT conformational analysis of diethyl 2-[(3-fluorophenylamino)methylene]malonate (**P1**), dimethyl 2-[(3-fluorophenylamino)methylene]malonate (**P2**), and 3-[(3-fluorophenylamino)methylene]pentane-2,4-dione (**P3**) push–pull compounds<sup>19</sup> is reported, focusing presumably on fluorine in position 3 (C3–F) (see Table 1). The outcome of the conformational analysis is critically confronted with the obtained X-ray structures. In addition, to obtain a better insight on the conformational behavior of the molecules (especially for the *trans* ethyl ester group of **P1** compound), the method of molecular dynamics (MD) is utilized. Consequently, the theoretical investigation of conformational analysis, vibrational spectra, electronic transitions, and NMR chemical shifts are presented. The obtained results are analyzed with respect to

Table 2. Crystal Data of the Precursors under Study

precursor	P1	P2	P3
empirical formula	C <sub>14</sub> H <sub>16</sub> FNO <sub>4</sub>	C <sub>12</sub> H <sub>12</sub> FNO <sub>4</sub>	C <sub>12</sub> H <sub>12</sub> FNO <sub>2</sub>
formula weight (g mol <sup>-1</sup> )	281.28	253.23	221.23
temperature (K)	100(1)	293(2)	293(2)
wavelength (Å)	0.71073	0.71073	0.71073
crystal system, space group	triclinic, <i>P</i> $\bar{1}$	triclinic, <i>P</i> $\bar{1}$	triclinic, <i>P</i> $\bar{1}$
unit cell dimension	<i>a</i> = 8.7649(5) Å <i>b</i> = 8.7954(7) Å <i>c</i> = 9.007(1) Å $\alpha$ = 90.566(9)° $\beta$ = 95.610(8)° $\gamma$ = 100.043(6)°	<i>a</i> = 7.1117(3) Å <i>b</i> = 7.1194(4) Å <i>c</i> = 12.0150(7) Å $\alpha$ = 74.345(5)° $\beta$ = 85.823(4)° $\gamma$ = 79.083(4)°	<i>a</i> = 6.1162(3) Å <i>b</i> = 9.6371(5) Å <i>c</i> = 10.2412(5) Å $\alpha$ = 108.298(4)° $\beta$ = 98.083(4)° $\gamma$ = 100.432(4)°
volume (Å <sup>3</sup> )	680.15(12)	575.01(5)	550.90(5)
<i>Z</i> , calc density (mg m <sup>-3</sup> )	2, 1.373	2, 1.463	2, 1.334
absorption coefficient (mm <sup>-1</sup> )	0.109	0.121	0.102
<i>F</i> (000)	296	264	232
crystal size (mm <sup>3</sup> )	0.689 × 0.222 × 0.072	0.998 × 0.533 × 0.166	0.961 × 0.790 × 0.092
$\theta$ range for data collection (deg)	4.115 to 26.371	4.525 to 24.713	4.098 to 24.702
reflections collected/unique	7910/2637	14108/1952	7308/1865
completeness to 2 $\theta$ = 25.00	95.9%	96.1%	95.8%
refinement method	full-matrix least-squares on <i>F</i> <sup>2</sup>		
data/restraints/parameters	2637/0/191	1952/0/165	1865/133/147
GoF on <i>F</i> <sup>2</sup>	1.041	1.032	1.044
final <i>R</i> indices [ <i>I</i> > 2 $\sigma$ ( <i>I</i> )]	<i>R</i> 1 = 0.0534 <i>wR</i> 2 = 0.1284	<i>R</i> 1 = 0.0354 <i>wR</i> 2 = 0.0953	<i>R</i> 1 = 0.0413 <i>wR</i> 2 = 0.1099
<i>R</i> indices (all data)	<i>R</i> 1 = 0.0683 <i>wR</i> 2 = 0.1398	<i>R</i> 1 = 0.0388 <i>wR</i> 2 = 0.0986	<i>R</i> 1 = 0.0505 <i>wR</i> 2 = 0.1172
$\Delta\rho_{\max}$ and $\Delta\rho_{\min}$ (e Å <sup>-3</sup> )	0.357 and -0.302	0.237 and -0.200	0.149 and -0.181

the experimentally measured spectra and the obtained crystal structures.

## EXPERIMENTAL METHODS

Crystallization of **P1** precursor was performed via a slow diffusion between a double layer of water (antisolvent) into dimethyl sulfoxide (**P1** containing solution). **P2** precursor was crystallized out of chloroform by a slow diffusion of vapors of antisolvent (hexane). Crystals of **P3** were prepared by a slow evaporation of solvent from the mixture of chloroform/methanol in ratio 10:1 (vol). All crystals of the studied precursors were colorless, and the precipitation took 1 week. X-ray diffraction data were collected on Oxford Diffraction Gemini R diffractometer equipped with Ruby CCD detector and Mo K $\alpha$  sealed-tube source at 100 or 293 K. Data collection and reduction was performed with Oxford Diffraction CrysAlis PRO version 1.171.37.31.<sup>31</sup> Crystal structures were solved by direct methods with SHELXS-2008 and refined by least-squares procedure on *F*<sup>2</sup> with SHELXL-2013.<sup>32</sup> DIAMOND was used for the molecular graphics.<sup>33</sup>

IR spectra in the region of 4000–700 cm<sup>-1</sup> were recorded on the Nicolet model NEXUS 470 FT-IR spectrometer. The FT-IR spectra in CHCl<sub>3</sub> were measured in Omni-cell assembling with KBr liquid Omni windows with lead spaces. The UV–vis spectra of the investigated compounds in CHCl<sub>3</sub> and dimethyl sulfoxide (DMSO) were recorded using a UV–vis–NIR UV 3600 spectrophotometer (Shimadzu, Japan) with a 1 cm square quartz cell. All NMR spectra were measured on the Agilent 600 MHz VNMRs spectrometer operating at frequencies 600 and 150 MHz for <sup>1</sup>H, <sup>19</sup>F, and <sup>13</sup>C nuclei and on an Agilent 300 MHz VNMRs spectrometer operating at frequencies 300 and

75 MHz for <sup>1</sup>H, <sup>19</sup>F, and <sup>13</sup>C nuclei. All details of FT-IR, UV–vis, and NMR measurements are described in Plevová et al.<sup>19</sup>

## COMPUTATIONAL DETAILS

The geometry optimization was performed at the B3LYP<sup>34–37</sup>/6-311++G\*\*<sup>38</sup> level of theory using Gaussian03.<sup>39</sup> Solvent effects in DMSO and CHCl<sub>3</sub> solutions were approximated by the integral equation formalism polarizable continuum model (IEFPCM),<sup>40,41</sup> and a full conformational analysis of the fluoroquinolone precursors under study was performed. A vibrational analysis was used to confirm that the optimal geometry corresponds to the energy minimum (no imaginary vibrations) and to obtain the vibrational spectra. TD-DFT electronic transitions<sup>42,43</sup> were computed for each relevant conformer using the same solvent as in the experimental measurements (DMSO and CHCl<sub>3</sub>). The 50 lowest electron excitations from the ground state were accounted for. <sup>13</sup>C, <sup>1</sup>H, and <sup>19</sup>F NMR chemical shifts were calculated using the individual gauges for atoms in molecules (IGAIM)<sup>44,45</sup> and the gauge-including atomic orbital (GIAO)<sup>46–49</sup> approaches as embedded in Gaussian 03. TMS (<sup>1</sup>H and <sup>13</sup>C NMR) and CFCl<sub>3</sub> (<sup>19</sup>F NMR) were employed as NMR standards in the determination of theoretical chemical shifts. Atomic charges from the quantum theory of atoms in molecules<sup>50–52</sup> have been obtained from the AIMAll package.<sup>53</sup> The molecular dynamics (MD) in vacuo calculations of **P1** precursor were performed at the B3LYP/6-311G\*\* level of theory using NWChem.<sup>54</sup> A Berendsen thermostat<sup>55</sup> was employed, and the temperature was set to 300 K with a time step of 0.001 ps. The optimized ZZa **P1** conformer was used as the starting geometry in the MD simulation because of the higher Boltzmann ratio

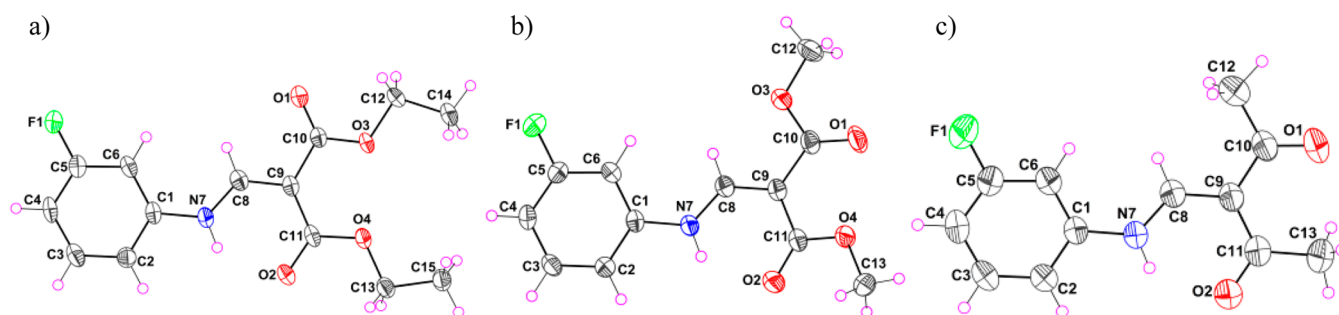


**Figure 2.** ORTEP drawing of (a) **P1** (disordered F2 and H5A atoms were omitted) (b) **P2** and (c) **P3** showing the labeling of the nonhydrogen atoms with 50% probability thermal displacement ellipsoids.

(approximately 85% in vacuo, see Table 4). The full time duration of the MD simulation at 300 K was 16.5 ps.

## RESULTS AND DISCUSSION

**X-ray Structure.** ORTEP format drawings of the **P1–P3** precursors (data shown in Table 2) are shown in Figure 2. All compounds (**P1–P3**) crystallize in the triclinic  $P\bar{1}$  space group with one molecule in the asymmetric unit. The **P1** compound is in the ZZa conformation in the crystal, where the fluorine atoms are disordered in the ratio of 88:12 with respect to the 5 to 3 position in the benzene ring, respectively. Structures of **P2** and **P3** are in the EZa conformation, and the fluorine atom is in the position 5. The comparison of the experimental and theoretical geometries will be discussed within the section on theoretical results.

Intra- and intermolecular hydrogen bonds play an important stabilizing role in the studied structures (**P1–P3**) in the solid state. Dominant feature of each structure is the strong intramolecular hydrogen bond between the N7 and O2 atoms of the amino and carbonyl groups creating a six-membered ring (Table 3). Additional intermolecular C–H...O

interactions are also observed (see Table S-1 of the Supporting Information). These interactions form one-dimensional (1D) (**P1**), two-dimensional (2D) (**P3**), or three-dimensional (3D) (**P2**) chains in the particular crystal structures as shown in Figure S-1 of the Supporting Information.

**Conformational Analysis.** The outcome of the B3LYP/6-311++G\*\*/IEFPCM conformational analysis of the studied **P1–P3** compounds is compiled in Table 4. Only the anti conformers of the studied precursors are considered (*syn* conformers are not energetically favored and hence omitted from any further discussion). The Boltzmann ratios of the EEa and ZEa conformers are less than 3%; thus, these conformers and their properties are for brevity left out from any further discussions.

Following the obtained results, the impact of the substituents on the conformational ratios of the precursors under study is substantial (Table 4). Apparently, the acetyl group is preferring the EZa conformer (**P3** precursor), while the ethyl ester substituted **P1** precursor prefers the ZZa conformer, regardless of the solvent model inclusion. Thus, the different ratios for the **P1** and **P3** precursors can be assigned to the different contribution of the mesomeric or induction effects (push–pull  $\pi$ -conjugation) and the steric repulsion effects of the particular substituents. In this respect, the intramolecular hydrogen bond between the oxygen of C=O (ester or acetyl group) and the hydrogen of the N–H group as well as the degree of electron density delocalization are also to be mentioned. Conversely, the Boltzmann ratio of the methyl ester substituted **P2** is significantly affected by the inclusion of the solvent effects in comparison with **P1**. This discrepancy can

**Table 3.** Intramolecular Hydrogen-Bond Geometry Parameters for Precursors ( $\text{\AA}$ , deg) Obtained from X-ray

precursor	D–H...A	$d(\text{D–H})$	$d(\text{H...A})$	$d(\text{D...A})$	$\angle(\text{DHA})$
<b>P1</b>	N7–H7...O2	0.86	1.97	2.636(2)	132.8
<b>P2</b>	N7–H7...O2	0.86	2.02	2.670(1)	131.6
<b>P3</b>	N7–H7...O2	0.86	1.96	2.608(2)	131.4

**Table 4.** Total Energy Difference  $\Delta E$ , Relative Population (Boltzmann Ratio) at Room Temperature and Total Dipole Moment of the Systems under Study with Fluorine in Position 3 (C3–F)

		$\Delta E$ (kJ mol <sup>−1</sup> )			Boltzmann ratio (%)			Total dipole moment (D)		
		gas	CHCl <sub>3</sub>	DMSO	gas	CHCl <sub>3</sub>	DMSO	gas	CHCl <sub>3</sub>	DMSO
<b>P1</b>	EEa	22.95	14.03	8.56	0	0	2	4.4751	6.8122	8.0425
	EZa	4.28	4.56	3.45	15	24	19	2.4690	3.6287	4.2307
	ZEa	15.07	12.13	9.45	0	1	2	2.0310	3.4980	4.2883
	ZZa	0.00	0.00	0.00	85	75	77	1.5908	1.5684	1.8085
<b>P2</b>	EEa	22.59	12.21	7.05	0	0	3	4.5448	6.7241	7.8369
	EZa	3.41	0.94	0.00	20	40	53	2.5846	3.9355	4.5814
	ZEa	15.24	9.36	7.23	0	2	3	2.0727	3.3267	3.9514
	ZZa	0.00	0.00	0.60	80	58	41	1.0692	0.9160	0.8504
<b>P3</b>	EEa	43.74	17.11	30.67	0	0	0	5.8353	9.6334	9.3264
	EZa	0.00	0.00	0.00	92	89	89	4.3790	5.9473	6.6529
	ZEa	37.40	30.39	26.37	0	0	0	4.0673	5.8301	6.5281
	ZZa	5.97	5.17	5.28	8	11	11	0.8630	1.4112	1.8259



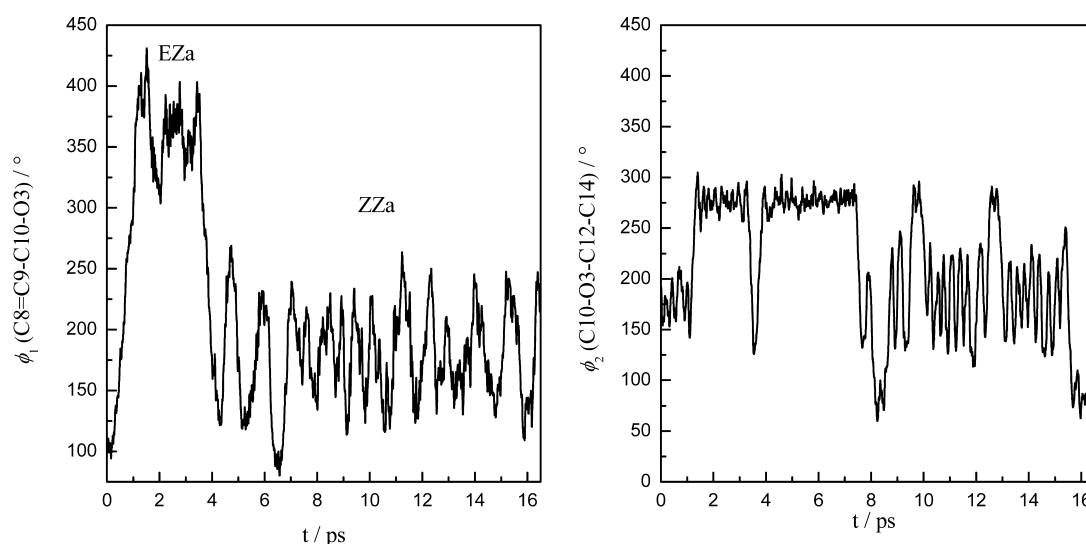


**Figure 3.** Time evolution of chosen dihedral angles of the MD B3LYP/6-311G\*\* (300 K) simulation: (a) EZa and ZZa transition and (b) orientation for the *trans* ethyl ester group.

be attributed to a different contribution of the aforementioned effects. In accordance with Table 4, the EZa:ZZa Boltzmann ratio of **P2** in vacuo is approximately 1:4, while in  $\text{CHCl}_3$  and DMSO, the ratios change to 2:3 and 1:1, respectively.<sup>30</sup>

The major difference in the geometry of **P1**, **P2**, and **P3** compounds is found for the intramolecular hydrogen N–H···O bond (see Table S-2). Decrease in the O···H bond length in **P3**, compared with the corresponding values for **P1** and **P2**, can be assigned to the repulsion of the methyl moieties of the acetyl groups causing bending of the acetyl oxygen toward the hydrogen of the amine.

The actual difference in the dipole moments of the EZa and ZZa conformers and their dependence on the solvent polarity is another factor, which can be related to the EZa:ZZa Boltzmann ratios (see Table 4). The difference in the in vacuo dipole moments of the EZa and ZZa conformers is the largest for **P3**. This can be closely related to that found in vacuo ratio, where **P3** prefers the EZa conformer, while **P1** and **P2** do prefer the ZZa one. The same trend between the value of dipole moments and EZa:ZZa ratio has also been found in the  $\text{NH}_2\text{--C}\equiv\text{C--}(\text{COCH}_3)_2$  in vacuo study at B3LYP and MP2 levels of theory.<sup>29</sup> In addition, one finds a considerable variation of total dipole moments of the studied precursors with respect to the solvent effects (and/or solvent polarity). Although the dipole moment of EZa conformers is always increasing with the inclusion and/or polarity of the solvent for all studied precursors **P1–P3**, the dependence of the dipole moment of ZZa conformers upon the solvent inclusion/polarity do vary among the studied precursors (see Table 4). From a qualitative prospective, the increase in the dipole moment should increase the cavitation energy, leading to a lower total energy due to larger electrostatic interactions with the cavity. In the case of EZa and ZZa conformers of **P3**, the increase in dipole moments with the polarity of the solvent leads to a similar change in total energies. Hence, the Boltzmann ratios are staying almost constant for **P3** irrespective of the solvent type. In the case of **P2**, the dipole moment of the EZa (ZZa) conformer is increasing (decreasing) with the polarity of the solvent, which lowers (raises) the total IEFPCM energy. Thus, EZa conformer population of **P2** becomes increased with the solvent inclusion/polarity. In the case of **P1**, the dipole moment of ZZa (EZa)

conformer for  $\text{CHCl}_3$  is decreasing (increasing). Thus, EZa conformer of **P1** should be more stabilized by the IEFPCM  $\text{CHCl}_3$  solvent model comparing to the ZZa conformer. Nevertheless, the energetic stabilization of EZa conformer of **P1** in  $\text{CHCl}_3$  is smaller ( $1.51 \text{ kJ mol}^{-1}$  relative to ZZa), comparing to **P2** ( $2.47 \text{ kJ mol}^{-1}$  relative to ZZa). In the DMSO solvent, the increase in the dipole moment of both conformers of **P1**, EZa and ZZa, is qualitatively in accordance with the small shift of the Boltzmann ratio toward the ZZa conformer.

From the topological point of view, the only significant change in the QTAIM charges for the different conformers/precursors is found for the hydrogen on C8 of **P3** EZa conformer (see Table S-3 of the Supporting Information). In any case, the ZZa conformers have only one hydrogen bond (characterized by the existence of a BCP) for the N–H···O moiety (see Table S-4 of the Supporting Information), while in the case of EZa conformers of **P1** and **P2**, a C8–H···O labile hydrogen bond (and/or the BCP) with the oxygen of the ester group is also found (see Table S-4 of the Supporting Information).

The position of the fluorine atom can also be considered as an additional conformational degree of freedom. The meta position of fluorine on the phenyl ring can be labeled 3 or 5 with respect to rotation around the C1–N7 axis; atom labels are following the notation in Table 1. It is found that the position of fluorine does not significantly affect the total energy and hence the EZa:ZZa ratios of **P1**. The ZZa:EZa 5-fluoro conformers ratio for  $\text{CHCl}_3$  remains ca. 76:24 and for DMSO changes to 71:26 (EEa 2% and ZEa 1%), when comparing to the ratios of pure 3-fluoro conformers shown in Table 4. Hence, each **P1** conformer (preferably EZa and ZZa) can have the fluorine atom almost equally distributed in both positions. The same can be expected for the remaining precursors **P2** and **P3**. The impact of the position of fluorine on the electronic transitions or IR spectra of **P1** will be considered in the coming sections. Nevertheless, in the MD simulations of **P1**, the rotation of the phenyl ring did not occur (see below). On the other hand, the fluorine atom in the X-ray structures is in position 5 for **P2** and **P3** and/or is disordered in the case of the **P1** precursor.

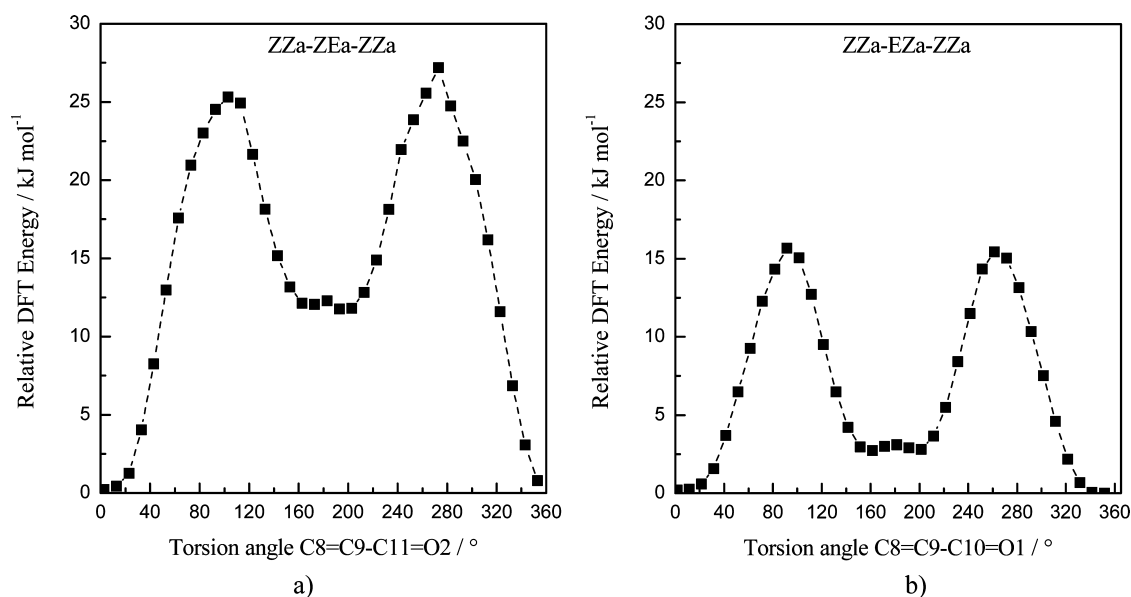


**Figure 4.** Dependence of the relative B3LYP/6-311++G\*\*/CHCl<sub>3</sub> energy of **P1** on the torsion angle: (a) *cis* ethyl ester group and (b) *trans* ethyl ester group.

Besides the fluorine position, the comparison of the calculated EZa:ZZa Boltzmann ratios with the obtained X-ray structures yields good agreement of the preferred conformation for **P1** and **P3** precursors (i.e., ZZa and EZa, respectively). In the case of **P2**, where the calculated Boltzmann ratio, including the solvent effects is approximately 1:1, the EZa conformer becomes preferred in the crystal structure. Whether this is to be assigned to a favorable packing for the EZa conformer of **P2** and/or to kinetic or thermodynamic effects goes beyond the scope of this study. As mentioned previously, the position of the fluorine atom becomes altered in the X-ray structures with respect to its position in the theoretical conformational analysis. Herein, the focus will be on the impact of the fluorine position on the spectral behavior of the studied species rather than on the full conformational analysis. Nevertheless, from the latter, no real impact of the position of the fluorine atom is found on the conformational analysis of **P1**.

The conformational analysis of the studied precursors is affected by several effects (i.e., push–pull  $\pi$ -conjugation, the steric repulsion effects of the particular substituents, the intramolecular hydrogen bond, or the hybridization of the nitrogen), which consequently also affect the Boltzmann ratios of the studied precursors. In order to further investigate the conformational behavior of the studied species, including the rotational degrees of freedom of the *trans* ethyl ester group for the ZZa conformer of **P1**, the fluorine position and the dynamics of the conformational changes, the additional MD simulations and conformational analyses of **P1** precursor were carried out.

The time dependences of two selected dihedral angles of **P1** from MD simulation are shown in Figure 3.  $\phi_1$  is related to the atoms C8=C9–C10–O3 (EZa/ZZa transition), and  $\phi_2$  is related to the C10–O3–C12–C14 atoms (orientation of the *trans* ethyl group as a further conformational degree of freedom). The starting ZZa conformation of **P1** is turning into the EZa conformer in the very beginning of the 300 K MD simulation (at ca. 0.2–1.0 ps) [see the orientation of the dihedral angle  $\phi_1$ (C8=C9–C10–O3) in Figure 3a]. After this transition, **P1** keeps the EZa conformation for approximately 3

ps of the MD simulation and then returns to the ZZa conformer for the rest of the simulation. In accordance with the data from the MD simulation in vacuo (represented by Figure 3a), the ZZa conformer is preferred for a significantly longer time (ca. 13 ps, which means approximately 79% of the total MD time). Following these results, the MD ratio between ZZa and EZa isomer is 4:1, which corresponds well with the calculated DFT Boltzmann ratio of **P1** precursor in DMSO (see Table 4). Nonetheless, the time duration of the MD simulation can be considered short to represent a full statistical ensemble, hand-in-hand with the fact that only one trajectory was studied.

Following the MD simulations, the dihedral angle  $\phi_2$ (C10–O3–C12–C14), and therefore the conformation of the whole *trans* ethyl ester group, is changing rather quickly (see Figure 3b). The energetically most populated torsion angle (180°, see also the global minimum in Figure 5) is kept in the beginning of the simulation and more or less in the time interval of 7.5–15.5 ps, as well. Nevertheless, during the first part of the MD simulation (i.e., time = 1.5–7.5 ps), the torsion angle of about 280° is preferred, which corresponds to one of the two saddle points of the possible orientation of the *trans* ethyl group (see also the coming paragraph and/or Figure 5). The second saddle point (related to the torsion angle of ca. 100°, see Figure 5) appears only briefly in the MD trajectory, particularly around 8.5 and 16 ps. Dependence of the relative DFT energy on  $\phi_1$  and  $\phi_2$  torsion angles will be further discussed in the coming paragraph. The time dependences of complementary dihedral angles (particularly C11–O4–C13–C15, C8=C9–C11=O2, and C8–N7–C1–C2) obtained from the MD simulation are provided in Figures S-2, S-3, and S-4 of the Supporting Information. The larger amplitude of oscillations of torsion angle  $\phi_2$  around 180° comparing to 280° or 100° can be assigned to the shape of the DFT energy dependence on  $\phi_2$ , as shown in Figure 4. The particular energy curve is broader at the global minimum at 180° comparing to the saddle points (see the following paragraph). The most characteristic motion of the ester groups of **P1** during the MD simulation is the change in the O1=C10–C9–C11 dihedral angle (with energetical

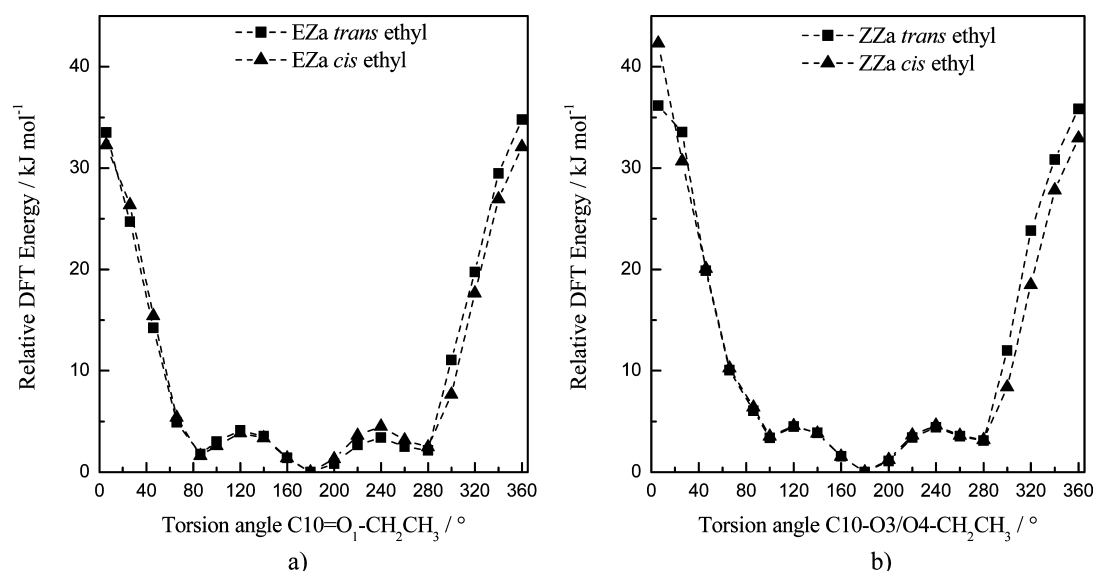


Figure 5. Dependence of the relative B3LYP/6-311++G\*\*/CHCl<sub>3</sub> energy of **P1** on the torsion angle: (a) *cis* ethyl group and (b) *trans* ethyl group.

Table 5. Characteristic B3LYP/6-311++G\*\*/CHCl<sub>3</sub> IR Line Spectra ( $\nu_{\text{calc}}$ ) (Scale Factor 0.9673<sup>56</sup>) of C3–F Precursors/Conformers and Experimental FT-IR Spectra ( $\nu_{\text{obs}}$ )<sup>19</sup> in CHCl<sub>3</sub> (in cm<sup>−1</sup>)

fundamental vibrations	P1			P2			P3		
	$\nu_{\text{calc}}$		$\nu_{\text{obs}}$	$\nu_{\text{calc}}$		$\nu_{\text{obs}}$	$\nu_{\text{calc}}$		$\nu_{\text{obs}}$
	EZa	ZZa		EZa	ZZa		EZa	ZZa	
N–H stretch	3318	3316	3263 (w)	3316	3320	3270 (w)	3239	3249	3177 (w)
<i>trans</i> C=O stretch	1671	1647	1680 (m)	1674	1652	1696 (m)	1636	1638	1662 (m)
C=C stretch	1617	1602	1629 (m)	1619	1604	1658 (m)	1606	1598	1627 (m)
<i>cis</i> C=O stretch	1599	1593	1599 (m)	1602	1601	1607 (m)	1586	1579	1607 (m)
C=C stretch	1581	1592	1591 (s)	1598	1593	1590 (m)	1577	1553	1581 (s)
C–F stretch	1207	1200	1192 (m)	1213	1202	1217 (s)	1217	1217	1190 (m)
=C–R <sup>a</sup> stretch	1228	1229	1267 (s)	1279	1276	1305 (m)	1229	1228	1247 (s)

<sup>a</sup>R = N, H; s, strong; m, medium; w, weak.

barrier estimated to  $\sim 4$  kJ mol<sup>−1</sup>). Following Figure S-4 of the Supporting Information, the dihedral angle for the benzene ring oscillates between 120–240°, which means that fluorine remains in position 3, while the experimental X-ray structure is disordered with respect to the position of fluorine in the case of **P1** (in the cases of **P2** and **P3**, the X-ray structures prefer position 5 of fluorine).

In spite of the obtained MD results, the dependence of the relative DFT energy of **P1** for the transition between the conformers ZZa  $\rightarrow$  ZEa  $\rightarrow$  ZZa (by the rotation of the *cis* ethyl ester group) and ZZa  $\rightarrow$  ZEa  $\rightarrow$  ZZa (by the rotation of the *trans* ethyl ester group) has been investigated. These dependencies are depicted in Figure 4. It can be immediately seen that the rotational barrier is twice as large for the *cis* ethyl ester group (due to breaking of the N–H $\cdots$ O hydrogen bond) as for the *trans* ethyl ester group. The relative energies of EZa and ZEa conformers of **P1** can be found in Table 4. The mutual orientation of the *trans* ethyl group ( $\phi_2$ ) represents a further factor which enters following the MD simulations the conformational behavior of the **P1** precursor.

The dependence of the relative DFT energy on the dihedral angle  $\phi_2$ (C10–O3–C12–C14) is given in Figure 5. This comparison represents a critical test for the conformational analysis of **P1**, since geometries with different torsional orientation of ethyl groups have been detected in the presented

MD simulations. The calculated DFT energy dependences on the particular dihedral angle for EZa and ZZa conformers of **P1** exhibit one minimum and two saddle points. The corresponding energy barriers are in the case of ZZa conformer 3.2 and 3.5 kJ mol<sup>−1</sup> and for the EZa conformer 1.8 and 2.5 kJ mol<sup>−1</sup>. Nevertheless, the additional degree of freedom of the possible orientation of ethyl group is affecting the overall Boltzmann populations of **P1** in the same manner, thus leaving the Boltzmann ZZa:ZEa ratio unaffected. In addition, theoretical calculations of **P1** have shown that these three different orientations of the ethyl groups do not influence the final spectra and chemical shifts at all. In the case of IR spectra of **P1**, the most influenced is the C=C vibration (by about 5 cm<sup>−1</sup>). Other characteristic vibrations are affected by less than 2 cm<sup>−1</sup>.

On the other hand, the maximum in UV–vis spectra in CHCl<sub>3</sub> were found unaffected for all possible ethyl group orientations of EZa and ZZa conformers of **P1**. The NMR chemical shifts are shifted by maximum 1 ppm. Thus, we are presenting the electronic transitions, IR line spectra, and NMR chemical shifts of the most stable EZa and ZZa conformers for all studied precursors.

**Infrared Spectra.** Table 5 shows the calculated and experimental<sup>19</sup> N–H, C=O, C=C, and C–F characteristic vibrations in CHCl<sub>3</sub>. In general, the unscaled theoretical harmonic vibrational frequencies are larger than the funda-



Table 6. Calculated (calc) and Experimental (obs)<sup>19</sup> Absorption Maximum Wavelengths (in nm) with the Oscillator Strength of the Most Populated Conformers<sup>a</sup>

precursor		CHCl <sub>3</sub>			DMSO		
		$\lambda_{\text{max, obs}}$	$\lambda_{\text{max, calc}}$	oscillator strength	$\lambda_{\text{max, obs}}$	$\lambda_{\text{max, calc}}$	oscillator strength
P1	EZa	319	310 (313)	0.8323 (0.8195)	318	310 (310)	0.8360 (0.8620)
	ZZa		314 (320)	0.8467 (0.8412)		313 (318)	0.8504 (0.8375)
P2	EZa	318	310	0.8226	318	309	0.8240
	ZZa		313	0.8079		313	0.8113
P3	EZa	336	327	0.0576	335	322	0.3175
			320	0.6892		316	0.4317
	ZZa		332	0.5444		329	0.6193
			321	0.1473		316	0.0724

<sup>a</sup>The calculated absorption maximum with the oscillator strengths of P1 conformers with fluorine position 5 are given in parentheses.

mentals observed experimentally. A major source of this disagreement is the neglected anharmonicity or the missing solvent–solute interactions within the theoretical treatment. Additional errors also arise from an incomplete incorporation of electron correlation and the use of finite basis sets. The relatively uniform nature of the overestimation of quantum chemical harmonic vibrational frequencies for a particular theoretical procedure allows the application of generic frequency scale factors. In accordance with Merrick et al.,<sup>56</sup> we used the scale factor of 0.9673.

The free N–H stretching vibration band in IR spectra is expected to be found around 3500 cm<sup>−1</sup>. Nevertheless, it is necessary to take into account the existence of the hydrogen bond in the studied EZa and ZZa conformers. Thus, for the N–H···O moiety, the N–H stretching vibration is shifted down to around 3340–3300 cm<sup>−1</sup>, as found for P1 and P2 (see Table 5). These particular N–H stretching vibrations for ZZa conformers of P1 and P2 are assigned to the scaled B3LYP/6-311++G\*\*/CHCl<sub>3</sub> modes at 3316 and 3320 cm<sup>−1</sup>, respectively. In the case of P3, the N–H stretching vibration is found below 3300 cm<sup>−1</sup>. This N–H mode of P3 (3239 cm<sup>−1</sup>) is found at slightly lower wavenumbers due to the stronger intramolecular hydrogen bond than for the dimethyl diethyl ester analogues, which is in light with the shorter N–H···O bond distance in P3.

In general, aliphatic and aromatic carboxylic acid esters are characterized by three intense infrared bands which lie in the ranges around 1700, 1200, and 1100 cm<sup>−1</sup>. This so-called “three band rule”<sup>57</sup> is diagnostic for the carboxylic acid ester group. Primarily, the band with the highest wavenumber will be considered; this band is formally assigned to the C=O stretching mode (although coupling with other modes often occurs). For the studied compounds, the C=O stretching vibrations are usually found in the range of 1700–1600 cm<sup>−1</sup>. The P1 and P2 precursors have a very similar frequencies of the highest *trans* C=O stretching vibration for the ZZa or EZa conformers. For instance, the ZZa conformers of the *trans* ethyl and methyl esters have this highest band at 1647 and 1652 cm<sup>−1</sup>, respectively. The *trans* C=O stretching vibration of the acetyl group P3 is shifted to lower wavenumbers comparing to P1 and P2. The *cis* C=O vibration of the ethyl ester group in P1 is found at 1593 cm<sup>−1</sup> and for the methyl ester group in P2 at 1601 cm<sup>−1</sup>. Thus, a very strong impact when comparing the frequency of the *cis* and *trans* C=O modes can be assigned to the intramolecular hydrogen bond. The impact of the strong intramolecular hydrogen bond on the assignment of the *cis* and *trans* C=O stretching vibrations can also be seen in the case of the P3 precursor (two acetyl groups). Bands at 1636 and 1586

cm<sup>−1</sup> can be assigned to the *trans* and *cis* C=O (acetyl) stretching vibration of P3, respectively.

Vibrations at 1602 and 1576 cm<sup>−1</sup> of P1 ZZa conformer correspond to C=C vibrations of the  $\pi$ -conjugated push–pull system (including coupling of the aromatic ring and C=C bond vibrations with the in-plane vibration of the N–H bond). These vibrations are coupled to each other, therefore, it is not possible to assign a specific wavenumber to a specific vibrational mode directly. Similarly, the vibration at 1228 cm<sup>−1</sup> consists of the carbon stretching vibration C<sub>||</sub>–O (hydrogen bond) and the C<sub>||</sub>–N vibration. A very similar situation is found for the EZa conformer of P1 and the EZa/ZZa conformers of P2 and P3 (see Table 5).

As was mentioned in the previous section, the *meta* position of fluorine in the phenyl ring can be labeled as 3 or 5 with respect to the rotation around the C1–N7 axis. For the ZZa conformer of P1, the calculated C3–F vibration can be found at 1200 cm<sup>−1</sup>, and for P1 conformers with fluorine position 5 is the C5–F vibration at 1230 cm<sup>−1</sup>. Thus, the fluorine position has no real influence on the frequencies of the considered vibration. In addition, the C–F vibration with fluorine in position 3 is in better agreement with the experimental value for P1.

**TD-DFT Electronic Transitions.** Following the experimentally measured UV–vis spectra, the characteristic absorption band of the studied precursors is found in the range of 300–350 nm.<sup>19</sup> This transition can be formally assigned to the  $n \rightarrow \pi^*$  (HOMO→LUMO) excitation in the  $\alpha$ ,  $\beta$ -unsaturated carbonyl chromophore (C <sub>$\alpha$</sub> =C <sub>$\beta$</sub> –C=O) containing two coupled carbonyl centers.<sup>58</sup> The experimental<sup>19</sup> and calculated absorption maxima and the oscillator strengths are summarized in Table 6.

In order to evaluate the electronic transitions of the studied P1–P3 precursors, the TD-DFT B3LYP/6-311++G\*\*/CHCl<sub>3</sub>/DMSO level of theory has been utilized. The ZZa (EZa) conformers of P1 and P2 reveal very similar TD-DFT/CHCl<sub>3</sub> absorption maxima at 314 and 313 nm (310 nm), respectively. In the calculated absorption spectra, the maximum absorption wavelengths for P1 and P2 correspond to the electronic transition from HOMO to LUMO (this transition was dominant in the expansion of the TD-DFT wave function). The highest bathochromic effect in the experimental UV–vis spectra is found for P3.<sup>19</sup> Moreover, the experimental spectral band for P3 is much broader.<sup>19</sup> The EZa conformer of P3 has actually two TD-DFT absorptions which have to be taken into account (especially for the DMSO solvent) and which can explain the broadening in the measured UV–vis spectra. (The highest transitions of the EZa and ZZa conformers of P3

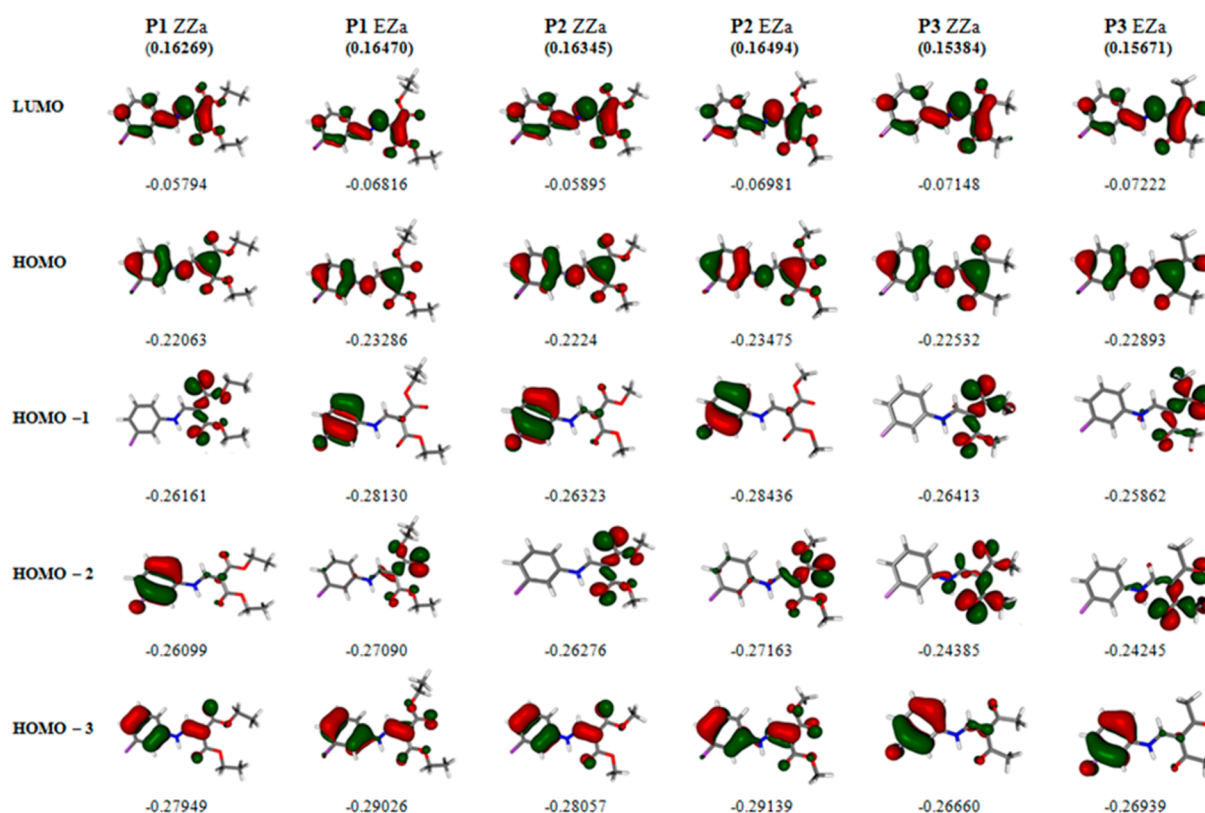


**Figure 6.** B3LYP/6-311++G\*\*/CHCl<sub>3</sub> frontier orbitals and orbital energies of the EZa/ZZa conformers of the studied compounds **P1–P3**. Values in parentheses represent the HOMO–LUMO gaps;  $\Delta E = E_{\text{LUMO}} - E_{\text{HOMO}}$  (all values are in Hartree).

**Table 7.** <sup>13</sup>C NMR IGAIM B3LYP/6-311++G\*\* and Experimentally Obtained (obs)<sup>19</sup> Chemical Shifts (in ppm) of Investigated Precursors in DMSO (**P1**) and in CHCl<sub>3</sub> (**P2** and **P3**)

		C1	C2	C3	C4	C5	C6	C8	C9	CO	CH <sub>2</sub>	CH <sub>3</sub>
<b>P1</b>	EZa	115.2	109.1	171.8	114.1	147.2	137.4	156.1	97.3	176.5	66.9	16.4
										170.6	64.6	15.8
	ZZa	114.8	108.6	171.8	113.1	146.6	137.3	156.1	96.7	176.0	67.1	15.9
										174.9	66.8	15.9
<b>P2</b>	EZa	113.4	104.3	162.7	110.8	141.3	131.2	150.5	94.2	167.0	59.7	14.1
										164.7	59.5	14.1
	ZZa	114.7	108.8	171.6	112.9	146.8	136.6	155.4	96.4	176.6	—	53.6
										170.2	—	53.3
<b>P3</b>	EZa	114.5	108.3	171.6	112.5	146.5	136.6	155.6	96.9	176.3	—	53.5
										174.4	—	53.7
	ZZa	112.9	104.4	163.6	111.4	140.7	131.2	151.7	93.8	169.2	—	51.7
										165.7	—	51.5
<b>P3</b>	EZa	113.6	109.9	171.6	115.8	146.7	136.7	156.5	115.5	210.0	—	36.6
										201.5	—	28.7
	ZZa	113.1	109.2	171.5	113.1	146.2	136.6	154.6	118.2	205.8	—	33.0
										203.7	—	32.3
<b>P3</b>	obs	113.5	104.9	163.5	112.6	140.7	131.3	151.2	113.6	201.3	—	32.0
										194.9	—	27.3

involve besides HOMO to LUMO also HOMO–1 to LUMO transitions).

From Figure 6, it can be seen that although the shapes of all HOMO and LUMO orbitals are very similar to each other, the LUMO orbital energies of **P3** precursor are shifted from **P1** and **P2** LUMO orbital energies, what may explain the bathochromic shift of **P3**. Furthermore, the HOMO–1 energies of **P3** are also shifted from the particular orbital energies of **P1** and **P2** which can be related to the occurrence of the second

(HOMO–1 to LUMO) transition in the calculated TD-DFT spectra of **P3**. Note also that the order and orbital energies are varying for HOMO–1 to HOMO–3 for **P1–P3** compounds (see Figure 6) (orbitals below HOMO–3 are not considered).

**NMR Spectra.** The experimental and IGAIM <sup>13</sup>C NMR and <sup>1</sup>H NMR/<sup>19</sup>F NMR chemical shifts are presented in Tables 7 and 8, respectively. Results from the IGAIM and GIAO methods give qualitatively satisfactory results with respect to the experiment, when considering the <sup>1</sup>H and <sup>13</sup>C NMR

**Table 8.**  $^1\text{H}$  and  $^{19}\text{F}$  NMR IGAIM B3LYP/6-311++G\*\* and Experimentally Obtained (obs) $^{19}\text{F}$  Chemical Shifts (in ppm) of Investigated Precursors in DMSO (P1) and in  $\text{CHCl}_3$  (P2 and P3)

		F	aromatic	CH	NH	CH <sub>2</sub>	CH <sub>3</sub>
P1	EZa	−185.8	6.26–6.95	7.58	9.22	3.76	1.08
						3.80	0.83
	ZZa	−186.1	6.19–6.93	7.43	9.28	3.66	1.08
						3.75	1.04
	obs	−111.7	6.96–7.20	8.36	10.65	4.12	1.24
P2	EZa	−185.9	6.12–6.79	7.49	9.41	—	3.06
						—	3.21
	ZZa	−186.3	6.08–6.80	7.45	9.30	—	3.10
						—	3.17
	obs	−111.8	6.81–7.31	8.46	11.01	—	3.78
P3	EZa	−185.1	6.18–6.82	7.21	10.94	—	1.69
						—	1.75
	ZZa	−185.1	6.10–6.81	7.25	10.68	—	1.55
						—	1.81
	obs	−111.7	6.88–7.40	8.18	12.71	—	2.38
						—	2.54

chemical shifts. In the following, only the IGAIM theoretical chemical shifts will be considered further; GIAO chemical shifts are presented in Tables S-5 and S-6 for completeness. As can be seen from Table 8, chemical shifts of  $^{19}\text{F}$  are grossly underestimated. Nevertheless, the tendency to underestimate the magnetic shieldings of halogenated groups at the B3LYP level of theory has been reported previously by Bauduin et al.,<sup>59</sup> for instance. The differences between the observed and calculated  $^{19}\text{F}$  NMR chemical shifts are possibly steaming from the missing spin–orbit effects<sup>60</sup> and the lack of electron correlation.<sup>61</sup> The impact of the fluorine position (3 vs 5) on the  $^{19}\text{F}$  chemical shift is only 1 ppm in the case of the ZZa P1 precursor.

The calculated  $^1\text{H}/^{13}\text{C}$  chemical shifts are often quantitatively under- or overestimated in comparison to the experimental values. Thus, the total chemical shifts are not really suited for describing the conformational behavior of the studied precursors quantitatively. However, the difference of the  $^{13}\text{C}$  chemical shifts between *cis* and *trans* carbons (CO, CH<sub>2</sub>, CH<sub>3</sub>) of the ester and/or acetyl moieties are worth being considered in this respect (the particular chemical shifts are shown in Table 7). These differences for the *cis* versus *trans* CO, CH<sub>2</sub>, CH<sub>3</sub> carbons of the ZZa conformer of P1 are in quantitative agreement with the differences for the observed chemical shifts, confirming the ZZa conformer as preferred. Consequently,  $\Delta\delta_{\text{obs}}(\text{CO})$  equals 2.3 ppm, the theoretical EZa shift  $\Delta\delta_{\text{EZa}}(\text{CO})$  is 5.9 ppm, and the theoretical ZZa shift  $\Delta\delta_{\text{ZZa}}(\text{CO})$  is 1.1 ppm and is considerably closer to  $\Delta\delta_{\text{obs}}(\text{CO})$ . The differences between the observed *cis* and *trans* chemical shifts of CO and CH<sub>3</sub> carbons lie between the differences of the calculated EZa and ZZa conformers of P2. This is in agreement with the conformational analysis, suggesting almost equal population of both conformers. Similarly, for P3, the observed and calculated differences in chemical shifts of CO and CH<sub>3</sub> carbons point to the EZa conformer.

The differences between the particular *cis* and *trans* CH<sub>2</sub> and CH<sub>3</sub>  $^1\text{H}$  NMR shifts of a given conformer and the experimental

results correlate well with the results of the conformational analysis for P1 (the particular chemical shifts are shown in Table 8). In the cases of P2 and P3, the differences between the experimental *cis* and *trans* chemical shifts of CH<sub>3</sub> are less satisfactory with respect to the results of the conformational analysis. Worse correlation for the differences in the  $^1\text{H}$  theoretical and experimental chemical shifts, with respect to the conformational analysis, can be mainly related to the small magnitude of the particular differences of  $\Delta\delta$ .

## CONCLUSIONS

The presented B3LYP/6-311++G\*\* conformational analysis of 3-fluorophenylamino methylene derivatives has confirmed that in the gas phase P1 and P2 precursors prefer the ZZa while P3 prefers the EZa conformation. On the other hand, the theoretical calculations in the solvent showed that the three studied fluoroquinolone precursors can prefer EZa, ZZa, or both conformers for P3, P1, and P2, respectively. Differences in the dipole moments for the EZa and ZZa conformers are reflecting the found EZa:ZZa Boltzmann ratios for both in vacuo and in-solvent calculations. Finally, the MD simulation has indeed revealed the dynamical changes between EZa and ZZa conformers of P1 as well as the rotational degree of freedom of the ethyl group of the ester of P1. The impact of the ethyl group rotation on the Boltzmann ratio or spectral characteristics of P1 is negligible. X-ray structures are in good agreement with the energetically preferred conformers of P1 and P3 precursors. In the case of P2, the EZa conformer becomes preferred in the crystal structure, although the theoretical “in solution” EZa:ZZa Boltzmann ratio is approximately 1:1. Position of the fluorine atom becomes altered in the X-ray structures with respect to its position in the theoretical conformational analysis. Nevertheless, the 180° degree rotation of the benzene ring (i.e., the exchange of the fluorine position) was not observed in the short MD simulation of P1, and the impact of the fluorine position on the spectral behavior is found negligible, even for C–F vibration and or  $^{19}\text{F}$  chemical shifts.

The theoretically obtained IR line spectra show good correlation with experimentally observed FT-IR spectra. The stretching *trans* C=O vibration of the ester carbonyl group (in P1 and P2) is higher than for the acetyl group (in P3); the values are in the range of 1630–1680  $\text{cm}^{-1}$ . The *cis* C=O vibrations are similar for all three compounds and are shifted to lower wavenumbers due to the participation in the hydrogen bond. In addition, the different character of the substituent (P3 comparing to character P1 and P2) causes a blue shift of the experimental UV–vis absorption maxima, including the broadening of the absorption peak as is confirmed in the TD-DFT calculations. The correlation between the calculated and observed  $^1\text{H}$  and  $^{13}\text{C}$  chemical shifts is found reasonably good. On the contrary, the calculated  $^{19}\text{F}$  chemical shifts are considerably underestimated.<sup>60,61</sup> Especially, the differences in  $^{13}\text{C}$  chemical shifts between the *cis* and *trans* CO, CH<sub>2</sub>, and CH<sub>3</sub> groups of the preferred conformer agree well with the observed differences in the particular experimental chemical shifts.

## ASSOCIATED CONTENT

### Supporting Information

Packing in the crystal structures including intermolecular hydrogen bonds of the studied precursors (a) P1, (b) P2,



and (c) **P3** (Figure S-1). Time evolution of dihedral angle C11–O4–C13–C15 of the B3LYP/6-311G\*\* MD simulation of the **P1** conformer (Figure S-2). Time evolution of dihedral angle C8=C9–C11=O2 of the B3LYP/6-311G\*\* MD simulation of the **P1** conformer (Figure S-3). Time evolution of dihedral angle C8–N7–C1–C2 of the B3LYP/6-311G\*\* MD simulation of **P1** conformer (Figure S-4). Observed versus calculated  $^{13}\text{C}$  NMR chemical shifts and  $^1\text{H}$  NMR chemical shifts of studied precursors obtained by the IGAIM and GIAO methods including the particular correlation coefficient (Figure S-5). Intermolecular hydrogen bonds in X-ray structures for all studied precursors, interatomic distances and bond angle ( $^\circ$ ) (Table S-1). Selected atomic distances ( $\text{\AA}$ ) in the conformers under study via B3LYP/6-311++G\*\* (Table S-2). Chosen B3LYP/6-311++G\*\*/ $\text{CHCl}_3$  QTAIM atomic charges of EZa/ZZa conformers of **P1**, **P2**, and **P3** precursors (Table S-3). Selected B3LYP/6-311++G\*\*/ $\text{CHCl}_3$  BCP characteristics [electron density ( $\rho_e$ ), Laplacian ( $\nabla^2$ ), and ellipticity ( $\epsilon$ )] of EZa/ZZa conformers of **P1**, **P2**, and **P3** precursors (Table S-4).  $^{13}\text{C}$  NMR GIAO B3LYP/6-311++G\*\* and experimentally obtained (obs) $^{19}$  chemical shifts (in ppm) of investigated precursors in DMSO (**P1**) and in  $\text{CHCl}_3$  (**P2** and **P3**) (Table S-5).  $^1\text{H}$  and  $^{19}\text{F}$  NMR IGAIM B3LYP/6-311++G\*\* and experimentally obtained (obs) $^{19}$  chemical shifts (in ppm) of investigated precursors in DMSO (**P1**) and in  $\text{CHCl}_3$  (**P2** and **P3**) (Table S-6). The complete author list of ref 1. The complete author list of ref 2. The complete author list of ref 39. The complete author list of ref 54. This material is available free of charge via the Internet at <http://pubs.acs.org>.

## AUTHOR INFORMATION

### Corresponding Author

\*E-mail: [lukas.bucinsky@stuba.sk](mailto:lukas.bucinsky@stuba.sk).

### Notes

The authors declare no competing financial interest.

## ACKNOWLEDGMENTS

The authors are grateful to E. Klein and Prof. A. Gatil (STUBA, Slovak Republic) for valuable comments on the manuscript, and M. Štjuber (STUBA, Slovak Republic) is greatly acknowledged for helpful discussions on the NMR data. This work was financially supported by the Research and Development Agency of the Slovak Republic under the Contracts APVV-0202-10, APVV-0339-10, and APVV-0038-11 and the Scientific Grant Agency (VEGA Project 1/0289/12 and 1/0829/14). The calculations were performed at HPC center, SUT Bratislava (SIVVP project, ITMS code 26230120002, funded by the European region development funds) and Computing Centre SAS, code 26210120002 (Slovak infrastructure for high-performance computing) supported by the Research & Development Operational Program funded by the ERDF.

## REFERENCES

- (1) Ma, Z.; Chu, D. T. W.; Cooper, C. S.; Li, Q.; Fung, A. K. L.; Wang, S.; Shen, L. L.; Flamm, R. K.; Nilius, A. M.; Alder, J. D.; et al. Synthesis and Antimicrobial Activity of 4H-4-Oxoquinolizine Derivatives: Consequences of Structural Modification at the C-8 Position. *J. Med. Chem.* **1999**, *42*, 4202–4213.
- (2) Santos, F. D. C.; Abreu, P.; Castro, H. C.; Paixão, I. C. P. P.; Cirne-Santos, C. C.; Giongo, V.; Barbosa, J. E.; Simonetti, B. R.; Garrido, V.; Bou-Habib, D. C.; et al. Synthesis, Antiviral Activity and

Molecular Modeling of Oxoquinoline Derivatives. *Bioorg. Med. Chem.* **2009**, *17*, 5476–5481.

- (3) Darque, A.; Dumètre, A.; Hutter, S.; Casano, G.; Robin, M.; Pannecouque, C.; Azas, N. Synthesis and Biological Evaluation of New Heterocyclic Quinolones as Anti-Parasite and Anti-HIV Drug Candidates. *Bioorg. Med. Chem. Lett.* **2009**, *19*, 5962–5964.

- (4) Madrid, P. B.; Sherrill, J.; Liou, A. P.; Weisman, J. L.; Derisi, J. L.; Guy, R. K. Synthesis of Ring-Substituted 4-Aminoquinolones and Evaluation of Their Antimalarial Activities. *Bioorg. Med. Chem. Lett.* **2005**, *15*, 1015–1018.

- (5) Hooper, D. C. Fluoroquinolone Resistance Fluoroquinolone Resistance among Gram-Positive Cocci. *Drug Resist. Updates* **2002**, *2*, 530–538.

- (6) Cunha, B. a.; Qadri, S. M.; Ueno, Y.; Walters, E. a.; Domenico, P. Antibacterial Activity of Trovafloxacin against Nosocomial Gram-Positive and Gram-Negative Isolates. *J. Antimicrob. Chemother.* **1997**, *39* (Suppl B), 29–34.

- (7) Kern, W. V.; Steib-Bauert, M.; de With, K.; Reuter, S.; Bertz, H.; Frank, U.; von Baum, H. Fluoroquinolone Consumption and Resistance in Haematology-Oncology Patients: Ecological Analysis in Two University Hospitals 1999–2002. *J. Antimicrob. Chemother.* **2005**, *55*, 57–60.

- (8) Andersson, M. I.; MacGowan, A. P. Development of the Quinolones. *J. Antimicrob. Chemother.* **2003**, *51* (Suppl 1), 1–11.

- (9) Li, L.; Wang, H.-K.; Kuo, S.-C.; Wu, T.-S.; Mauger, A.; Lin, C. M.; Hamel, E.; Lee, K.-H. Antitumor Agents 155. Synthesis and Biological Evaluation of 3',6,7-Substituted 2-Phenyl-4-Quinolones as Antimicrotubule Agents. *J. Med. Chem.* **1994**, *37*, 3400–3407.

- (10) Yamashita, Y.; Ashizawa, T.; Morimoto, M.; Hosomi, J.; Nakano, H. Antitumor Quinolones with Mammalian Topoisomerase II Mediated DNA Cleavage Activity. *Cancer Res.* **1992**, *10*, 2818–2822.

- (11) Wang, J. C.; Lynch, S. Transcription and DNA Supercoiling. *Curr. Opin. Genet. Dev.* **1993**, *3*, 764–768.

- (12) Lhiaubet-vallet, V.; Bosca, F.; Miranda, M. A.; Valencia, D. Review Photosensitized DNA Damage: The Case of Fluoroquinolones. *Photochem. Photobiol.* **2009**, *85*, 861–868.

- (13) Song, C.; Ryu, H.; Park, J.; Ko, T. Mechanism of DNA Gyrase Inhibition by Quinolones: I. Spectral Analysis for Nalidixic Acid Polymorphism. *Bull. Korean Chem. Soc.* **1999**, *20*, 727–730.

- (14) Suzuki, I.; Takahashi, M.; Shigenaga, A.; Nemoto, H.; Takeda, K. Synthesis and Photo DNA-Damaging Activities of Fluoroquinolone Analogues. *Tetrahedron Lett.* **2006**, *47*, 6193–6196.

- (15) Emami, S.; Shafiee, E.; Foroumadi, A. Quinolones: Recent Structural and Clinical Developments. *Iran. J. Pharm. Res.* **2005**, *3*, 123–136.

- (16) Shen, L. L. A Reply: “Do Quinolones Bind to DNA?”—Yes. *Biochem. Pharmacol.* **1989**, *38*, 2042–2044.

- (17) Leyva, E.; Monreal, E.; Herna, A. Synthesis of Fluoro-4-Hydroxyquinoline-3-Carboxylic Acids by the Gould  $\pm$  Jacobs Reaction. *J. Fluor. Chem.* **1999**, *94*, 8–11.

- (18) Gould, R. G.; Jacobs, W. A. The Synthesis of Certain Substituted Quinolones and 5,6-Benzquinolones. *J. Am. Chem. Soc.* **1939**, *61*, 2890–2895.

- (19) Plevová, K.; Dorotíková, S.; Škodová, M.; Dvoranová, D.; Milata, V.; Kubincová, J.; Devínsky, F. Building a Combinatorial Library for Monofluorinated Anilinoethylenes and Their Spectral Studies. *Monatsh. Chem.* **2014**, accepted.

- (20) Rimarčík, J.; Lukeš, V.; Klein, E.; Kelterer, A.-M.; Milata, V.; Vrecková, Z.; Brezová, V. Photoinduced Processes of 3-Substituted 6-Fluoro-1,4-Dihydro-4-Oxoquinoline Derivatives: A Theoretical and Spectroscopic Study. *J. Photochem. Photobiol., A* **2010**, *211*, 47–58.

- (21) Rimarčík, J.; Punyain, K.; Lukeš, V.; Klein, E.; Dvoranová, D.; Kelterer, A.-M.; Milata, V.; Lietava, J.; Brezová, V. Theoretical and Spectroscopic Study of Ethyl 1,4-Dihydro-4-Oxoquinoline-3-Carboxylate and Its 6-Fluoro and 8-Nitro Derivatives in Neutral and Radical Anion Forms. *J. Mol. Struct.* **2011**, *994*, 61–69.

- (22) Kulhánek, J.; Bureš, F.; Mikýsek, T.; Ludvík, J.; Pytela, O. Imidazole as a Central II-Linkage in Y-Shaped Push–Pull Chromophores. *Dyes Pigm.* **2011**, *90*, 48–55.

- (23) Quist, F.; Vandavelde, C.; Didier, D.; Teshome, a; Asselberghs, I.; Clays, K.; Sergeyev, S. Push–Pull Chromophores Comprising Benzothiazolium Acceptor and Thiophene Auxiliary Donor Moieties: Synthesis, Structure, Linear and Quadratic Non-Linear Optical Properties. *Dyes Pigm.* **2009**, *81*, 203–210.
- (24) Kulhánek, J.; Bureš, F.; Pytela, O.; Mikysek, T.; Ludvík, J.; Růžicka, A. Push-Pull Molecules with a Systematically Extended  $\pi$ -Conjugated System Featuring 4,5-Dicyanoimidazole. *Dyes Pigm.* **2010**, *85*, 57–65.
- (25) Klaeboe, P. Infrared and Raman Spectroscopy Applied to Conformational Equilibria; Methods and Recent Results. *J. Mol. Struct.* **1997**, *408/409*, 81–89.
- (26) Klaeboe, P. Conformational Studies by Vibrational Spectroscopy: A Review of Various Methods. *Vib. Spectrosc.* **1995**, *9*, 3–17.
- (27) Smith, M. B.; March, J. *March's Advanced Organic Chemistry*; John Wiley & Sons, Inc.: Hoboken, NJ, 2006.
- (28) Bertolasi, V.; Gilli, P.; Ferretti, V.; Gilli, G. Intermolecular N–H...O Hydrogen Bonding Assisted by Resonance. II. Self Assembly of Hydrogen-Bonded Secondary Enaminones in Supramolecular Catemers. *Acta Crystallogr., Sect. B: Struct. Sci., Cryst. Eng. Mater* **1998**, *54*, 50–65.
- (29) Gróf, M.; Gatia, A.; Milata, V.; Prónayová, N.; Sümmchen, L.; Salzer, R. Conformational Studies of 3-Aminomethylene-2,4-Pentanedione Using Vibrational and NMR Spectra, and Ab Initio Calculations. *J. Mol. Struct.* **2007**, *843*, 1–13.
- (30) Gróf, M.; Gatia, A.; Matějka, P.; Kožíšek, J.; Milata, V.; Prónayová, N. Conformational Studies of Aminomethylene-Malonic Acid Dimethylester and Its N-Methyl Derivatives Using Vibrational Spectroscopy, X-Ray Analysis and Ab Initio Calculations. *J. Mol. Struct.* **2009**, *924–926*, 54–61.
- (31) *CrysAlisPro*, version 1.171.36.20; Oxford Diffraction Ltd.: Abingdon, Oxford, England, 2012.
- (32) Sheldrick, G. M. A Short History of SHELX. *Acta Crystallogr., Sect. A: Found. Crystallogr.* **2008**, *64*, 112–122.
- (33) Bergerhoff, G.; Berndt, M.; Brandenburg, K. Evaluation of Crystallographic Data with the Program DIAMOND. *J. Res. Natl. Inst. Stand. Technol.* **1996**, *101*, 221–225.
- (34) Becke, A. D. Density-functional Thermochemistry. III. The Role of Exact Exchange. *J. Chem. Phys.* **1993**, *98*, 5648–5652.
- (35) Stephens, P. J.; Devlin, F. J.; Chabalowski, C. F.; Frisch, M. J. Ab Initio Calculation of Vibrational Absorption and Circular Dichroism Spectra Using Density Functional Force Fields. *J. Phys. Chem.* **1994**, *98*, 11623–11627.
- (36) Vosko, S. H.; Wilk, L.; Nusair, M. Accurate Spin-Dependent Electron Liquid Correlation Energies for Local Spin Density Calculations: A Critical Analysis. *Can. J. Phys.* **1980**, *58*, 1200–1211.
- (37) Lee, C.; Yang, W.; Parr, R. G. Development of the Colle-Salvetti Correlation-Energy Formula into a Functional of the Electron Density. *Phys. Rev. B* **1988**, *37*, 785–789.
- (38) Krishnan, R.; Binkley, J. S.; Seeger, R.; Pople, J. A. Self-Consistent Molecular Orbital Methods. XX. A Basis Set for Correlated Wave Functions. *J. Chem. Phys.* **1980**, *100*, 12960–12973.
- (39) Frisch, M. J.; Trucks, G. W.; Schlegel, H. B.; Scuseria, G. E.; Robb, M. A.; Cheeseman, J. R.; Montgomery, Jr., J. A.; Vreven, T.; Kudin, K. N.; Burant, J. C.; et al. *Gaussian 03*, revision C.02; Gaussian, Inc.: Wallingford, CT, 2004.
- (40) Cossi, M.; Barone, V.; Mennucci, B.; Tomasi, J. Ab Initio Study of Ionic Solutions by a Polarizable Continuum Dielectric Model. *Chem. Phys. Lett.* **1998**, *286*, 253–260.
- (41) Cossi, M.; Barone, V.; Cammi, R.; Tomasi, J. Ab Initio Study of Solvated Molecules: A New Implementation of the Polarizable Continuum Model. *Chem. Phys. Lett.* **1996**, *255*, 327–335.
- (42) Bauernschmitt, R.; Ahlrichs, R. Treatment of Electronic Excitations within the Adiabatic Approximation of Time Dependent Density Functional Theory. *Chem. Phys. Lett.* **1996**, *256*, 454–464.
- (43) Laurent, A. D.; Jacquemin, D. TD-DFT Benchmarks: A Review. *Int. J. Quantum Chem.* **2013**, *113*, 2019–2039.
- (44) Keith, T. a.; Bader, R. F. W. Calculation of Magnetic Response Properties Using Atoms in Molecules. *Chem. Phys. Lett.* **1992**, *194*, 1–8.
- (45) Keith, T. a.; Bader, R. F. W. Calculation of Magnetic Response Properties Using a Continuous Set of Gauge Transformations. *Chem. Phys. Lett.* **1993**, *210*, 223–231.
- (46) Ruud, K.; Helgaker, T.; Bak, L. L.; Jensen, H. J. A. Hartree–Fock Limit Magnetizabilities from London Orbitals. *J. Chem. Phys.* **1993**, *99*, 3847–3859.
- (47) Ditchfield, R. Self-Consistent Perturbation Theory of Diamagnetism. *Mol. Phys.* **1974**, *27*, 789–807.
- (48) Woliński, K.; Sadlej, A. J. Self-Consistent Perturbation Theory. *Mol. Phys.* **1980**, *41*, 1419–1430.
- (49) Wolinski, K.; Hinton, J. F.; Pulay, P. Efficient Implementation of the Gauge-Independent Atomic Orbital Method for NMR Chemical Shift Calculations. *J. Am. Chem. Soc.* **1990**, *112*, 8251–8260.
- (50) Bader, R. F. W.; Nguyen-Dang, T. T. Quantum Theory of Atoms in Molecules–Dalton Revisited. *Adv. Quantum Chem.* **1981**, *14*, 63–124.
- (51) Bader, R. F. W. A Quantum Theory of Molecular Structure and Its Applications. *Chem. Rev.* **1991**, *91*, 893–928.
- (52) *The Quantum Theory of Atoms in Molecules: From Solid State to DNA and Drug Design*; Matta, C. F.; Boyd, R. J., Eds.; Wiley-VCH: Weinheim, 2007.
- (53) Keith, T. A. *AIMAll*, version 14.04.17; TK Gristmill Software: Overland Park, KS, 2014 (aim.tkgristmill.com).
- (54) Valiev, M.; Bylaska, E. J.; Govind, N.; Kowalski, K.; Straatsma, T. P.; van Dam, H. J. J.; Wang, D.; Nieplocha, J.; Apra, E.; Windus, T. L.; et al. NWChem: A Comprehensive and Scalable Open-Source Solution for Large Scale Molecular Simulations. *Comput. Phys. Commun.* **2010**, *181*, 1477–1489.
- (55) Berendsen, H. J. C.; Postma, J. P. M.; van Gunsteren, W. F.; DiNola, A.; Haak, J. R. Molecular Dynamics with Coupling to an External Bath. *J. Chem. Phys.* **1984**, *81*, 3684–3690.
- (56) Merrick, J. P.; Moran, D.; Radom, L. An Evaluation of Harmonic Vibrational Frequency Scale Factors. *J. Phys. Chem. A* **2007**, *111*, 11683–11700.
- (57) Reichenbacher, M.; Popp, J. *Challenges in Molecular Structure Determination*; Springer: Berlin, 2012.
- (58) Pretsch, E.; Bühlmann, P.; Affolter, C. *Structure Determination of Organic Compounds: Tables of Spectral Data*, 3rd ed.; Springer: Berlin, 2000.
- (59) Bauduin, G.; Boutevin, B.; Pitrasanta, Y. A Priori Calculation of Chemical Shifts in  $^{19}\text{F}$  NMR Spectroscopy. 4. Testing Our Model with New Experimental Values. *J. Fluor. Chem.* **1995**, *9*, 9–12.
- (60) Nakatsuji, H.; Nakajima, T.; Hada, M.; Takashima, H.; Tanaka, S. Spin-Orbit Effect on the Magnetic Shielding Constant Using the Ab Initio UHF Method: Silicon Tetrahalides. *Chem. Phys. Lett.* **1995**, *247*, 418–424.
- (61) Cheeseman, J. R.; Trucks, G. W.; Keith, T. A.; Frisch, M. J. A Comparison of Models for Calculating Nuclear Magnetic Resonance Shielding Tensors. *J. Chem. Phys.* **1996**, *104*, 5497–5509.